

Assimilation of Radar Radial Velocity Data with the WRF Hybrid Ensemble–3DVAR System for the Prediction of Hurricane Ike (2008)

YONGZUO LI, XUGUANG WANG, AND MING XUE

School of Meteorology and Center for Analysis and Prediction of Storms, University of Oklahoma, Norman, Oklahoma

(Manuscript received 8 February 2012, in final form 3 May 2012)

ABSTRACT

An enhanced version of the hybrid ensemble–three-dimensional variational data assimilation (3DVAR) system for the Weather Research and Forecasting Model (WRF) is applied to the assimilation of radial velocity (V_r) data from two coastal Weather Surveillance Radar-1988 Doppler (WSR-88D) radars for the prediction of Hurricane Ike (2008) before and during its landfall. In this hybrid system, flow-dependent ensemble covariance is incorporated into the variational cost function using the extended control variable method. The analysis ensemble is generated by updating each forecast ensemble member with perturbed radar observations using the hybrid scheme itself. The V_r data are assimilated every 30 min for 3 h immediately after Ike entered the coverage of the two coastal radars.

The hybrid method produces positive temperature increments indicating a warming of the inner core throughout the depth of the hurricane. In contrast, the 3DVAR produces much weaker and smoother increments with negative values at the vortex center at lower levels. Wind forecasts from the hybrid analyses fit the observed radial velocity better than that from 3DVAR, and the 3-h accumulated precipitation forecasts from the hybrid are also more skillful. The track forecast is slightly improved by the hybrid method and slightly degraded by the 3DVAR compared to the forecast from the Global Forecast System (GFS) analysis. All experiments assimilating the radar data show much improved intensity analyses and forecasts compared to the experiment without assimilating radar data. The better forecast of the hybrid indicates that the hybrid method produces dynamically more consistent state estimations. Little benefit of including the tuned static component of background error covariance in the hybrid is found.

1. Introduction

Tropical cyclones (TCs) are among the most costly forms of natural disaster (Pielke et al. 2008). An accurate TC forecast will require not only a numerical model to realistically simulate both the TC itself and its environment, but also a data assimilation (DA) system that can effectively use the observations to accurately estimate the initial TC vortex and the environment where the TC is embedded.

To address the TC initialization issue, many previous studies adopted the vortex relocation and/or bogussing (e.g., Liu et al. 2000; Kurihara et al. 1995; Zou and Xiao 2000) techniques. While such techniques are nontrivial and have been shown to improve the hurricane forecast, how to maintain the dynamical and thermodynamical

coherency of the hurricane and its environment is probably the biggest challenge with such methods.

Recently, several studies have explored the use of ensemble-based DA methods to initialize hurricane forecasts and have shown great promise (e.g., Torn and Hakim 2009; Zhang et al. 2009a; Li and Liu 2009; Hamill et al. 2011; Wang 2011; Weng et al. 2011; Zhang et al. 2011; Aksoy et al. 2012; Weng and Zhang 2012; Dong and Xue 2012). The key with ensemble-based DA is the use of an ensemble to estimate the forecast error statistics in a flow-dependent manner. Therefore, the observation information will be properly weighted and spread consistent with the background hurricane forecasts; and perhaps more importantly, the ensemble covariance can realistically infer the flow-dependent cross-variable error statistics and therefore update state variables not directly observed in a dynamically and thermodynamically consistent manner.

One candidate in ensemble-based DA is the hybrid ensemble-variational DA method. It has been proposed (e.g., Hamill and Snyder 2000; Lorenc 2003; Etherton

Corresponding author address: Yongzuo Li, Center for Analysis and Prediction of Storms, University of Oklahoma, 120 David L. Boren Blvd., Norman, OK 73072.
E-mail: yongzuo.li@ou.edu

and Bishop 2004; Zupanski 2005; Wang et al. 2007b, 2008a; Wang 2010), implemented, and tested with numerical weather prediction (NWP) models recently (e.g., Buehner 2005; Wang et al. 2008b; Liu et al. 2008, 2009; Buehner et al. 2010a,b; Wang 2011; Wang et al. 2011; Whitaker et al. 2011; Kleist et al. 2011; Wang et al. 2012, manuscript submitted to *Mon. Wea. Rev.*). A standard variational method (VAR) typically uses static background error covariance, but a hybrid ensemble-variational DA system incorporates ensemble-derived flow-dependent covariance into the VAR framework. The ensemble can be generated by an ensemble Kalman filter (EnKF). Recent studies have suggested that hybrid DA systems may represent the “best of both worlds” by combining the best aspects of the variational and EnKF systems (e.g., Buehner 2005; Wang et al. 2007a, 2008a,b, 2009; Zhang et al. 2009b; Buehner et al. 2010a,b; Wang 2010). While preliminary tests of the hybrid DA system with real NWP models and data have shown great potential of the method for non-TC forecasts (e.g., Wang et al. 2008b; Buehner et al. 2010a,b) and for forecasts of TC tracks (e.g., Wang 2011; Whitaker et al. 2011), and there has been a growing body of literature documenting the success of using the EnKF to assimilate inner-core data for TC initialization at convection-allowing resolutions (e.g., Zhang et al. 2009a; Weng et al. 2011; Zhang et al. 2011; Aksoy et al. 2012; Weng and Zhang 2012; Dong and Xue 2012), to the authors’ best knowledge, to date there is no published study applying a hybrid DA method to the assimilation of radar data at a convection-allowing resolution for TC predictions. This study serves as a pilot study applying the hybrid ensemble–three-dimensional variational data assimilation (3DVAR) system developed for the Weather Research and Forecasting Model (WRF) (Wang et al. 2008a) to explore its potential for assimilating radar observations for hurricane forecasts. As a first step of such a study, we focus on assimilating radar radial velocity data. Meanwhile, this study also performs detailed diagnostics to understand the fundamental differences between the roles and effects of flow-dependent and static covariances in the TC analysis and forecast.

More specifically, this study applies and explores the WRF ensemble–3DVAR hybrid system to the assimilation of coastal Weather Surveillance Radar-1988 Doppler (WSR-88D) radar radial velocity data for the prediction of Hurricane Ike (2008) (Fig. 1). Ike is the second costliest tropical cyclones in the recorded history (1900–2010) over the mainland United States (Blake et al. 2011). Previous studies (e.g., Zhao and Xue 2009) have shown significant impact of the radar data for this case using the Advanced Regional Prediction System

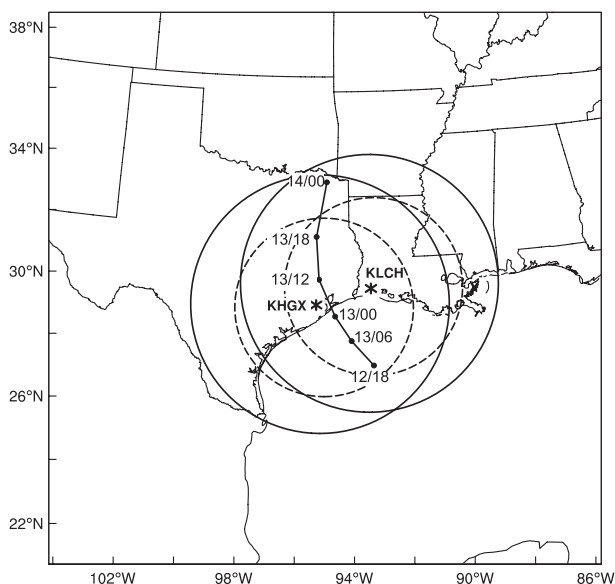


FIG. 1. The WRF domain and National Hurricane Center best-track positions for Hurricane Ike (2008) from 1800 UTC 12 Sep to 0000 UTC 14 Sep 2008. Also indicated are the Houston, Texas (KHGX), and Lake Charles, Louisiana (KLCH), WSR-88D radar locations (asterisks) and maximum range (300 km for the radial velocity and 460 km for the reflectivity) coverage circles.

(ARPS) 3DVAR/cloud analysis package. The remainder of this paper is organized as follows: section 2 presents the methodology and section 3 discusses the experiment design. The experiment results are discussed in section 4, while the final section summarizes the main conclusions of this study.

2. Methodology

The hybrid ensemble–3DVAR scheme

A diagram of the hybrid DA system is shown in Fig. 2. Similar to Hamill and Snyder (2000), the following four steps are repeated for each DA cycle: 1) Perform K (K is the ensemble size) number of ensemble forecasts to generate background forecast fields at the time of analysis. 2) Calculate ensemble forecast perturbations to be used by the hybrid cost function for flow-dependent covariance by subtracting ensemble mean from each member. 3) Generate K independent sets of perturbed observations by adding random perturbations to the observations. 4) Obtain the analysis increment for each ensemble member through minimization of the hybrid cost function using one set of perturbed observations. Steps 1 through 4 are repeated for each of the follow-on cycles, with the ensemble analyses providing initial conditions for step 1. In step 3, the random perturbations added to the observations are drawn from a Gaussian

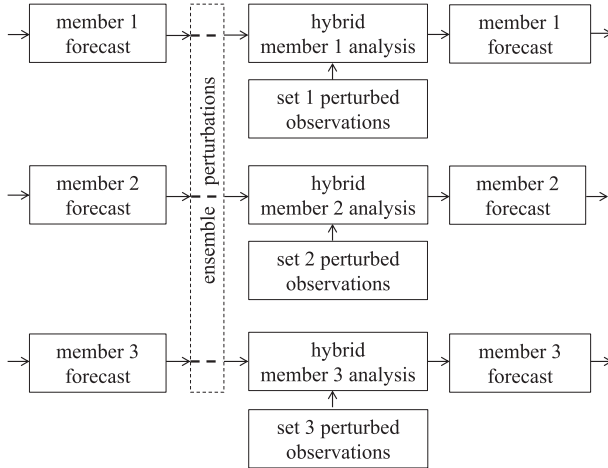


FIG. 2. Schematic diagram of the hybrid ensemble-3DVAR forecast-analysis cycle for a hypothetical three-member ensemble. Each member assimilates the observations containing a different set of perturbations.

distribution with a mean of zero and a standard deviation of the observation error. This “perturbed observation method” was used in Hamill and Snyder (2000), which corresponds to the classic stochastic ensemble Kalman filters (Burgers et al. 1998; Houtekamer and Mitchell 1998; Evensen 2003). In the original work of Wang et al. (2008a), the ensemble transform Kalman filter (ETKF) was used to update forecast perturbations.

A brief review on the extended control variable method for incorporating ensemble covariance into a WRF 3DVAR framework is given here. For detailed discussions, readers are referred to Wang et al. (2007b, 2008a).

For state vector \mathbf{x} , the analysis increment of the hybrid scheme \mathbf{x}' is the sum of two terms:

$$\mathbf{x}' = \mathbf{x}'_1 + \sum_{k=1}^K (\mathbf{a}_k \circ \mathbf{x}_k^e). \quad (1)$$

The first term \mathbf{x}'_1 in Eq. (1) is the increment associated with WRF 3DVAR static background covariance and the second term is the increment associated with flow-dependent covariance. Here, the vectors \mathbf{a}_k , $k = 1, \dots, K$, denote extended control variable (Lorenz 2003) for each ensemble member, and the second term of Eq. (1) represents a local linear combination of ensemble perturbations. The coefficient \mathbf{a}_k for each member varies in space as discussed later, which determines the ensemble covariance localization (see Wang et al. 2008a for further details). The variable \mathbf{x}_k^e is the k th ensemble perturbation state vector. The symbol “ \circ ” denotes the Schur product (element by element product) of the vectors \mathbf{a}_k and \mathbf{x}_k^e .

The cost function for WRF hybrid ensemble-3DVAR is

$$\begin{aligned} J(\mathbf{x}'_1, \mathbf{a}) &= \beta_1 J_b + \beta_2 J_e + J_o, \\ &= \beta_1 \frac{1}{2} (\mathbf{x}'_1)^T \mathbf{B}^{-1} (\mathbf{x}'_1) + \beta_2 \frac{1}{2} (\mathbf{a})^T \mathbf{A}^{-1} (\mathbf{a}) \\ &\quad + \frac{1}{2} (\mathbf{y}'^o - \mathbf{H}\mathbf{x}')^T \mathbf{R}^{-1} (\mathbf{y}'^o - \mathbf{H}\mathbf{x}'), \end{aligned} \quad (2)$$

where J_b is the traditional WRF 3DVAR background term associated with the static covariance \mathbf{B} and J_e is the hybrid term associated with flow-dependent covariance; \mathbf{a} is defined as $\mathbf{a}^T = (\mathbf{a}_1^T, \mathbf{a}_2^T, \dots, \mathbf{a}_K^T)$; and J_o is the observation term associated with observation error covariance \mathbf{R} . The innovation vector \mathbf{y}'^o is defined as, $\mathbf{y}'^o = \mathbf{y}^o - \mathbf{H}(\mathbf{x}^b)$, where \mathbf{y}^o is the observation vector, \mathbf{x}^b is the background forecast state vector, and \mathbf{H} is the linearized observation operator.

The weights of the static covariance and flow-dependent covariance are determined by factors β_1 and β_2 according to the following relationship:

$$\frac{1}{\beta_1} + \frac{1}{\beta_2} = 1, \quad (3)$$

which conserves the total variance.

As described in Wang et al. (2008a), the ensemble covariance localization, denoted as \mathbf{A} , has horizontal and vertical components. In this study, both the horizontal and vertical localization are applied. Specifically, the horizontal localization is modeled by a recursive filter transform as in Wang et al. (2008a). The vertical localization is implemented by transforming the extended control variable \mathbf{a} in Eq. (2) with empirical orthogonal functions (EOFs). The correlation matrix, denoted as Cov, from which the EOFs are derived, follows:

$$\text{Cov}(k_1, k_2) = \exp\left(-\frac{d^2}{L^2}\right), \quad (4)$$

where d is the distance between model levels k_1 and k_2 and L is the vertical localization radius. Existing EOF codes in the WRF 3DVAR for modeling the vertical static error covariance are used for the vertical ensemble covariance localization purpose.

3. Experimental design

a. The WRF model configuration

The Advanced Research WRF (ARW) version 3 (Skamarock et al. 2008) is used in this study. The model

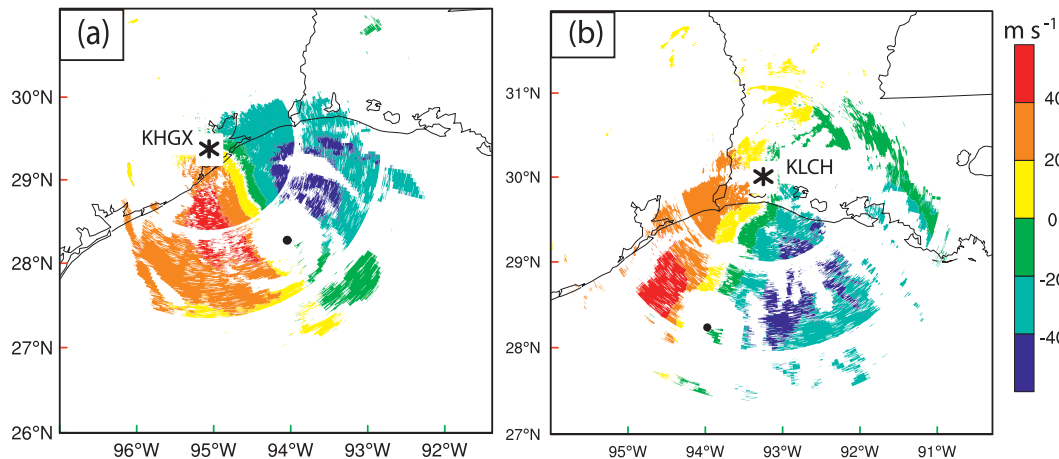


FIG. 3. The radial velocity (interval of 20 m s^{-1}) at 0.5° elevation angle from (a) KHGX and (b) KLCH WSR-88D radars at 0000 UTC 13 Sep 2008. The black dot is for NHC best-track position of Hurricane Ike (2008) at this time. Asterisks are for radar locations.

is compressible, three-dimensional, nonhydrostatic, discretized on an Arakawa C grid with terrain-following mass-based sigma coordinate levels. In this study, the WRF is configured with 401×401 horizontal grid points at 5-km grid spacing (Fig. 1), and 41 vertical levels with the model top at 100 hPa. The WRF Single-Moment 6-Class Microphysics scheme (WSM6; Hong et al. 2004) is chosen for the explicit microphysics processes. Since the grid resolution may not fully resolve the hurricane convective features, the Grell–Devenyi cumulus parameterization scheme (Grell and Devenyi 2002) is included. Other physics parameterizations schemes used include the Yonsei University (YSU; Noh et al. 2003) scheme for planetary boundary layer parameterization, the five-layer thermal diffusion model for land surface processes (Skamarock et al. 2008), the Rapid Radiative Transfer Model (RRTM) longwave (Mlawer et al. 1997), and the fifth-generation Pennsylvania State University–National Center for Atmospheric Research (PSU–NCAR) Mesoscale Model (MM5) shortwave (Dudhia 1989) radiation parameterization.

b. The radar data processing

The radial velocity data from coastal WSR-88D radars at Houston, Texas (KHGX), and Lake Charles, Louisiana (KLCH), are processed using a modified version of the four dimensional dealiasing algorithm (FDDA; James and Houze 2001). The algorithm was originally designed for Doppler radars in the European Alps. The modified algorithm by this study is capable of reading level-II WSR-88D data and dealiasing the radial velocities.

To dealias radial velocity data, the following steps are performed: first, a wind profile is created based on model

background, rawinsonde, or wind profiler data. The background radial velocity in radar observation space is calculated from the wind profile, assuming the wind is horizontally homogeneous. Second, the WSR-88D radial velocity is compared with the background radial velocity for a gross check. In this step, aliased radial velocity that needs to be corrected is identified. Third, at each elevation angle, spatial dealiasing is performed. The aliased velocity V_a will be recovered by factored Nyquist velocity V_n :

$$V_d = V_a + 2NV_n, \quad (5)$$

where N is a positive or negative integer whose sign and value are determined by a gate-to-gate shear threshold of $0.4V_n$ (James and Houze 2001). After dealiasing is finished, the radial velocity interpolated to the Cartesian coordinates is thinned to 10-km spacing horizontally and 500 m vertically.

Figure 3 shows the processed radial velocity at 0.5° elevation angle for KHGX (Fig. 3a) and KLCH (Fig. 3b) at 0000 UTC 13 September 2008. These two radars complement each other by providing scans that are approximately the right angle at the location of Ike's eye. KHGX covers almost all of Ike's eye and eyewall. The outbound radial velocity on the left side of the eye and inbound radial velocity on the right side of the eye reflect the circulation of the hurricane. KLCH covers only about half of the eye and eyewall. The outbound radial velocity on the front side of the eye and inbound radial velocity on the back side of the eye also reflect the circulation of the hurricane.

The observation error standard deviation for the radial velocity is set to 2 m s^{-1} during the DA. This error

TABLE 1. List of experiments.

Expt	Description
NoDA	No radar data assimilation. WRF initial condition interpolated from NCEP $1^\circ \times 1^\circ$ analysis
3DVARa	Radar DA using WRF 3DVAR with static covariance from NMC method
3DVARb	Same as 3DVARa, except the horizontal spatial correlation in the static covariance is multiplied by 0.3
HybridF	Radar DA using hybrid method with full weight given to flow-dependent covariance, with $1/\beta_1 = 1/1001$ and $1/\beta_2 = 1/1.001$ in Eq. (1)
HybridH	Hybrid method with equal weight given to static covariance (which is the same as 3DVARb) and flow-dependent covariance, with $1/\beta_1 = 1/2$ and $1/\beta_2 = 1/2$ in Eq. (1)

value is similar to the values used in Dowell and Wicker (2009), Xu and Gong (2003), and Xiao et al. (2009).

c. The data assimilation setup

This paper presents five experiments denoted as NoDA, 3DVARa, 3DVARb, HybridF, and HybridH (see definitions in Table 1). Experiments differ based on what, if any, assimilation system is used for radar data. The experiments are designed to examine the difference of using flow-dependent versus static background covariance when assimilating the radar data and the impact of DA on the subsequent forecast.

The NoDA experiment did not assimilate any radar data, instead the WRF initial condition at 0300 UTC 13 September 2008 simply comes from the $1^\circ \times 1^\circ$ National Centers for Environmental Prediction (NCEP) operational Global Forecast System (GFS) analysis. The 6-hourly GFS analyses also provide the lateral boundary conditions (LBCs).

The “3DVARb” experiment assimilated the radar data using the traditional 3DVAR method where the static background covariance is adopted. The static covariance is generated and further tuned as followed. The National Meteorological Center (NMC, now known as NCEP) method (Parrish and Derber 1992) was first employed to generate the static background covariance statistics based on 12- and 24-h WRF forecasts, starting at 0000 and 1200 UTC every day, during the period from 1 to 15 September 2008. The experiment using the static covariance generated by the above procedure without further tuning is denoted as 3DVARa. Because the default correlation length scales derived from the NMC method reflects mostly large-scale error structures, their direct use may not be appropriate for storm-scale radar DA (Liu et al. 2005). The horizontal correlation length scale of the static covariance is reduced by a factor of 0.3

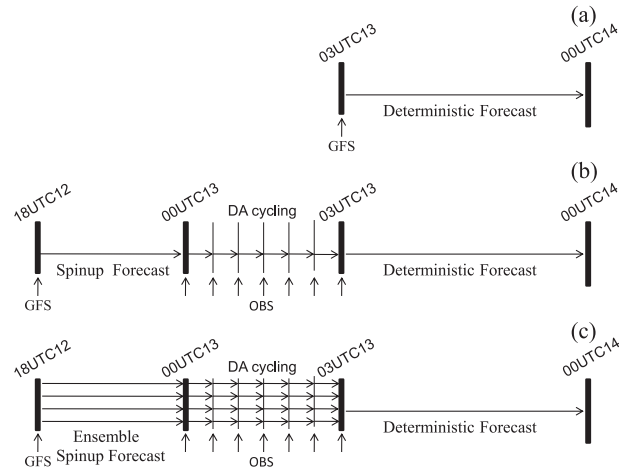


FIG. 4. The flow charts for (a) NoDA experiment, (b) 3DVAR experiments (3DVARa and 3DVARb), and (c) hybrid experiments (HybridF and HybridH).

in experiment 3DVARb and this factor is found to be optimal through experimentations. The 3DVAR experiments contain three stages (Fig. 4a). 1) A single 6-h spinup forecast initialized from the GFS analysis at 1800 UTC 12 September to produce an initial first guess at 0000 UTC 13 September for radar DA cycles. The spinup time of 6 h is based on past experiences and other published studies (e.g., Zhang et al. 2009a, spinup time of 9 h; Aksoy et al. 2012, spinup time of 6 h). 2) Assimilation of radial velocity data from KHGX and KLCH radars every 30 min for 3 h. 3) A 21-h deterministic forecast initialized by the analysis at the end of the assimilation cycles in step 2. The WRF boundary conditions for all three stages are also provided by the operational GFS analyses at 6-hourly intervals. Experiment 3DVARb serves as a base line for evaluating the performance of the hybrid method.

Experiments HybridF and HybridH are identical except that the different weighting factors β_1 and β_2 are used in Eq. (2). For HybridF, the full weight is assigned on the flow-dependent ensemble covariance (using $1/\beta_1 = 1/1001$ and $1/\beta_2 = 1/1.001$). For HybridH, the static covariance and the flow-dependent ensemble covariance are equally weighted ($1/\beta_1 = 1/2$ and $1/\beta_2 = 1/2$) (i.e., only half of the flow-dependent covariance is used, hence, the “H” in the name). The horizontal correlation scale of static covariance in HybridH is also reduced by a factor of 0.3 as in 3DVARb. Meanwhile, HybridH uses the same flow-dependent covariance localization as HybridF, which will be discussed in detail in section 4a.

Each of the hybrid experiments, HybridF and HybridH, has 40 ensemble members. Similar to the 3DVAR experiments, the hybrid experiments have three stages (Fig. 4b). 1) 6-h ensemble forecasts to spin up a first-guess

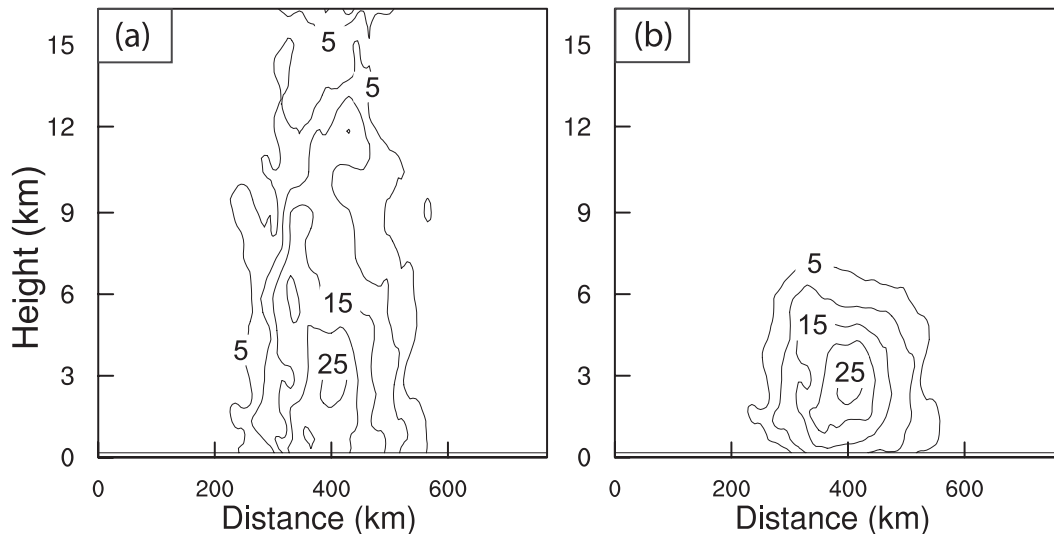


FIG. 5. The vertical cross section of the wind speed increment (interval of 5 m s^{-1}) using a single KHGX radar radial velocity data located at (28.4°N , 93.7°W ; 3176 m) with an innovation of -38.63 m s^{-1} using the configurations of experiment HybridF but (a) without and (b) with vertical localization at 0000 UTC 13 Sep 2008.

ensemble and provide flow-dependent covariance at the beginning of the radar DA cycles. The initial and boundary conditions for each member are the GFS analysis plus correlated random perturbations following Torn et al. (2006) and Wang et al. (2008a,b). 2) Assimilation of perturbed radial velocity data from KHGX and KLCH radars every 30 min for 3 h by variationally minimizing the hybrid cost function, according to the description given in the previous section (see also Fig. 2). 3) A 21-h deterministic forecast initialized from the ensemble mean analysis at the end of the DA cycles in step 2. To generate the random perturbations in step 1, the random-cv facility in the WRF 3DVAR system is employed (Barker et al. 2004). First, a random control variable vector is created with a normal distribution having a zero mean and unit standard deviation. Then the perturbation control variable vector is transformed to the model space to obtain perturbations to the model state variables including the horizontal wind components, pressure, potential temperature, and mixing ratio of water vapor. The perturbation standard deviations are roughly 1.9 m s^{-1} for the horizontal wind components, 0.6 K for temperature, 0.3 hPa for model pressure perturbation, and 0.9 g kg^{-1} for water vapor mixing ratio and these values are based on the NMC-method-derived background error statistics.

Like other ensemble-based data assimilation algorithm, the hybrid ensemble-3DVAR quickly reduces ensemble spread after assimilating observations. The relaxation method of Zhang et al. (2004) for ensemble covariance inflation was adopted. Specifically, the inflated

ensemble posterior perturbation \mathbf{x}'_{new} is a weighted average of prior perturbation \mathbf{x}'_f and posterior perturbation \mathbf{x}'_a , $\mathbf{x}'_{\text{new}} = (1 - b)\mathbf{x}'_f + b\mathbf{x}'_a$, the relaxation coefficient, denoted as b , is set to 0.5 in this study. This formulation retains part of prior perturbation to mitigate quick spread reduction.

4. Results and discussion

The analysis increment of the first DA cycle, the cycling process, the final analysis fields, and the deterministic forecasting results will be presented and discussed in this section. The subsection organization roughly follows the experiment flow charts in Fig. 4.

a. Single observation test for vertical localization

Before complete DA experiments are performed, the vertical covariance localization in the hybrid scheme is tested by assimilating a single radial velocity observation. Figure 5 shows the wind speed increment produced by HybridF analyzing a single radial velocity observation located 3176 m above sea level at 0000 UTC 13 September 2008. The innovation (i.e., the observed radial velocity minus forecast ensemble mean valid at 0000 UTC 13 September) for this observation is -38.63 m s^{-1} . Without the vertical localization, non-zero increment reaches the top of the model with relatively noisy increments at the upper levels (Fig. 5a). The horizontal and vertical localization radii of 60 and 3 km, respectively, are used in hybrid experiment HybridF (and in HybridH). The localization radii were empirically determined. For example, we tested 20, 60, 200, and 600 km

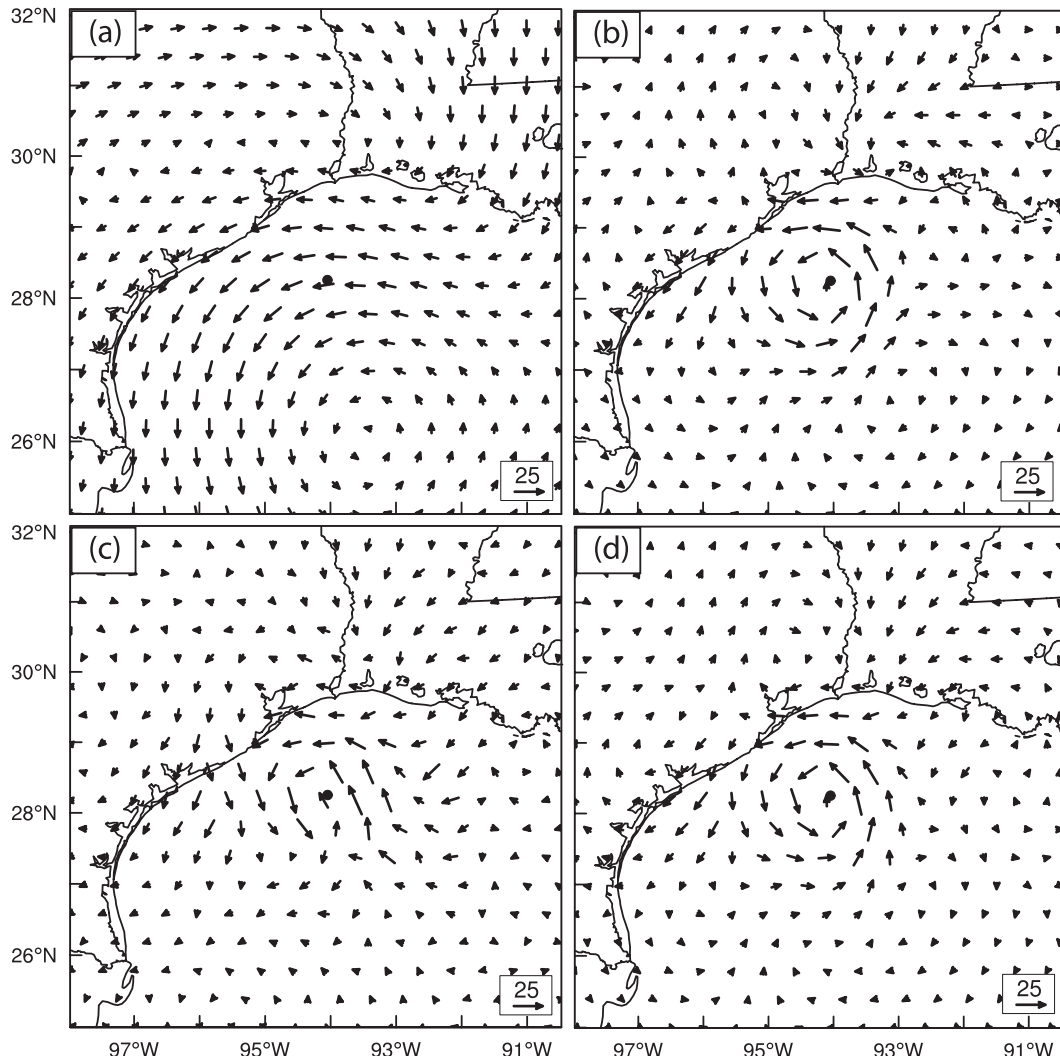


FIG. 6. The 700-hPa wind analysis increments (m s^{-1}) for (a) 3DVARa, (b) 3DVARb, (c) HybridF, and (d) HybridH at 0000 UTC 13 Sep 2008.

for horizontal localization and found the 60 km showed the most reasonable increment. The vertical localization was also tested. The radar observation over Ike's inner-core area is about 3 km above the surface. With 3-km vertical localization scale, the influence of radar data could reach the surface. Figure 5b shows that with such localizations, the analysis increment is more confined around the observation location. This single observation test shows that our implementation of the vertical localization is taking effect.

b. Wind increments

To see the differences in analyzing the radar data using flow-dependent and static covariances, the analysis increments from the 3DVAR and hybrid experiments after the first analysis time are compared. We first

look at the wind increments and will look at indirectly related cross-variable increments in the next subsection.

Figure 6 shows the wind analysis increments at 850 hPa, at 0000 UTC 13 September 2008, the time of first analysis for 3DVARa, 3DVARb, HybridF, and HybridH. The increment in 3DVARa using the default NMC-method-derived static covariance shows cyclonic and anticyclonic increment patterns of rather large scales (Fig. 6a); the cyclonic increment circulation is centered almost 2° off the observation hurricane center to the south-southeast, while at the hurricane center location the wind increment is mostly easterly. To the north the increment circulation shows an anticyclonic pattern. Such cyclonic and anticyclonic increments are also found in a previous studies assimilating radar radial velocity data using WRF 3DVAR (e.g., Xiao and Sun 2007), but

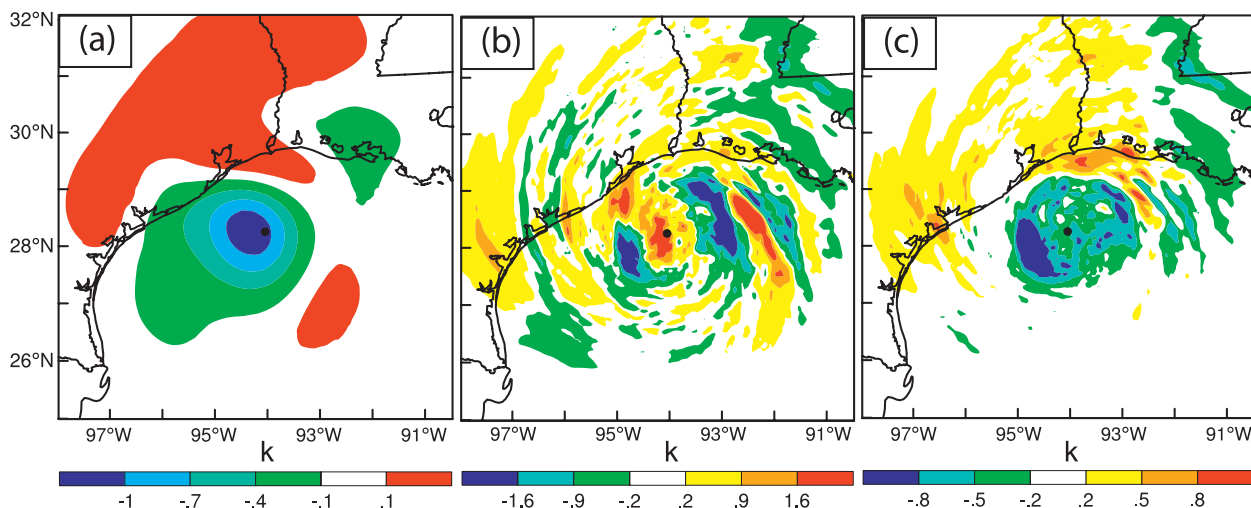


FIG. 7. The 850-hPa temperature analysis increments for (a) 3DVARb (at intervals of 0.3 K), (b) HybridF (at intervals of 0.7 K), and (c) HybridH (at intervals of 0.3 K), at 0000 UTC 13 Sep 2008.

are clearly unrealistic, and do not reflect the fact that a strong vortex exists where the background strongly underestimate the strength of the vortex. The default background error covariance derived from the NMC method is unaware of the hurricane vortex and its spatial correlation scales mostly reflect synoptic-scale error structures. The net result is the inappropriately large amount of smoothing of the radar data in the data-dense region and inappropriately large spreading of the information outside the data coverage region. The radar data, being collected at high spatial resolution, should be analyzed using much smaller spatial correlation scales. This had been pointed out in Liu et al. (2005). The use of smaller correlation scales for radar data is a common practice in the ARPS 3DVAR system (e.g., Hu et al. 2006; Schenkman et al. 2011). Sugimoto et al. (2009) also tested the sensitivity of WRF 3DVAR to the correlation length scale and the variance of the background covariance for radar data assimilation.

In 3DVARb, the default horizontal spatial correlation scale is reduced by a factor of 0.3. The resulting wind increment now shows a more or less symmetric cyclonic pattern around the observed center of Ike (Fig. 6b). Compared with 3DVARa, the large increments are more limited to the region of vortex in 3DVARb, and the increment is consistent with the inbound and outbound radial velocity couplets associated with the hurricane vortex as observed by KHGX and KLCH radars (Fig. 3). Such results are more realistic.

In HybridF with full weight given to the flow-dependent covariance, the wind increment also shows a cyclonic pattern centered around the eye of Ike (Fig. 6c), but the

increment circulation is less axisymmetric, reflecting the contribution of spatially inhomogeneous flow-dependent covariance. When equal weights are placed on the ensemble covariance and static covariance in HybridH, the wind increments show a pattern that is close to that of 3DVARb, but the increment magnitude is between those of the HybridF and 3DVARb (Fig. 6d).

c. Temperature increments

Because radar radial velocity is the only data type assimilated in this study, any increment in temperature is the result of balance relationship applied (if any) and/or due to cross covariance in the background error. Figure 7 shows the 850-hPa temperature increments for 3DVARb, HybridF, and HybridH after assimilating radial velocity data for the first cycle. For 3DVARb, negative temperature increments are found in the vortex region, and the magnitude is largest near the hurricane center (Fig. 7a). Physically, the enhanced hurricane vortex circulation should be accompanied by warming of the vortex core region, to give a warmer core vortex; hence, the 3DVAR temperature increment is inconsistent with expected hurricane structures. The negative increment is expected of the 3DVAR, because the increment is obtained through a balance relationship between temperature and wind and this relationship reflects the thermal wind relation. More specifically, the “balanced temperature” increment T_b at a vertical level k , in WRF 3DVAR is related to the streamfunction ψ by a regression relation, $T_b(k) = \sum_l G(l, k) \psi(l)$, where G is the regression coefficient and the summation is over the vertical index l . Such a regression relation derived using the NMC method generally reflects hydrostatic,

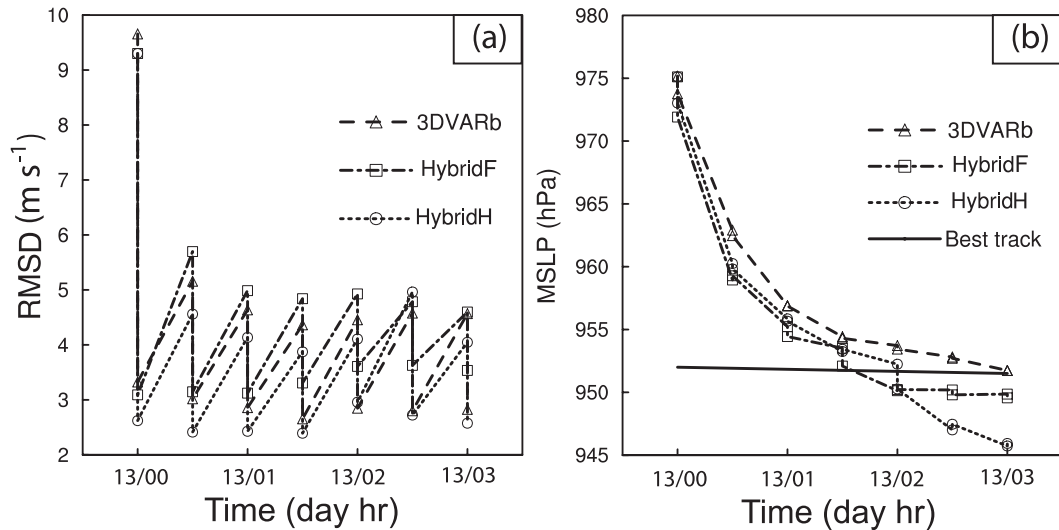


FIG. 8. The forecast and analysis (sawtooth pattern during DA cycling) of (a) RMSD of radial velocity (m s^{-1}), and (b) the minimum sea level pressures (hPa) together with the NHC best-track estimate, for 3DVARb, HybridF, and HybridH from 0000 to 0300 UTC 13 Sep 2008.

geostrophic, and thermal wind relations (Barker et al. 2004). A colder core at 850 hPa is consistent with an enhanced cyclonic circulation at 700 hPa seen in Fig. 6. Note that at this distance, the lowest radar beams do not reach below 850 hPa; hence, the enhancement of wind is larger above 850 hPa. Therefore the cyclonic wind increment increases with height in the lower atmosphere. We note that negative temperature increment is also seen in the low-level eye region of analyzed hurricanes in previous studies using Airborne Doppler radar data and WRF 3DVAR (e.g., Xiao et al. 2009).

Different from 3DVAR, the temperature increment obtained in HybridF shows positive increments in the eye region (Fig. 7b) and spiral patterns in the eyewall and outer rainband regions. In this case, the hurricane in the background forecast at 0000 UTC 13 September 2008 is much weaker than the observation (Fig. 8b), which is accompanied by lower temperatures at the core of the vortex than observed. When radar observations are assimilated, the background TC vortex is strengthened and therefore the core temperature is expected to be increased to be consistent with the warm core structure of TCs. The more realistic increment structures in HybridF are the result of temperature–wind cross covariances derived from the ensemble, which have knowledge of the vortex as a tropical cyclone. In addition, the magnitude of the temperature increments in HybridF is an order of magnitude larger than that of 3DVARb; the temperature increment in the 3DVAR analysis of Xiao et al. (2009) for Hurricane Jeanne (2004) was also weak, reflecting the relative weak thermal wind relationship in 3DVAR.

Same as the wind increment, the temperature increment from HybridH is in between those of HybridF and 3DVARb (Fig. 7c). The magnitude is about half that of HybridF. The structure of the increment resembles that of HybridF more, but the eye region has negative instead of positive increments. From this aspect, HybridH is poorer than HybridF.

d. Innovation statistics for V_r and minimum sea level pressure in DA cycles

The behaviors of 3DVARb, HybridH, and HybridF are further compared by examining the fit of their analyses and forecasts to V_r observations during the DA cycles. The fit is defined as the root-mean-square difference (RMSD) between the model state and observations, after the model state is converted to the observed quantities; and such difference is also called observation innovation. Figure 8 shows the RMSDs for V_r and minimum sea level pressure (MSLP) from HybridH, HybridF, and 3DVARb. The V_r data of both KHGX and KLCH are used in the innovation calculation and for the hybrid, the ensemble mean is used. In all three experiments, the RMSD for V_r is reduced significantly by the analysis within each cycle and the largest reduction occurs in the first analysis cycle at 0000 UTC when the observation innovations are the greatest. In later cycles, the innovations for the analyses remain roughly between 2.5 and 3.5 m s^{-1} , which is reasonable given the 2 m s^{-1} expected observation error. The 30-min forecasts following each analysis generally increase the V_r innovation by about 2 m s^{-1} , reaching 4–5 m s^{-1} levels. In general, HybridH produces analyses

that fit Vr observations tightest, while HybridF is the least and 3DVARb is in between. The same is true of the 30-min forecasts. Note that although the analysis increment of HybridH is in general (Figs. 6 and 7) in between HybridF and 3DVARb, the root-mean-square Vr fit to observations in HybridH is not necessarily between HybridF and 3DVARb. The observation innovation statistics can help us to see if the DA system is doing about the right things, but being “verification” against the same set of observations that is also used in the DA, it cannot really tell us the true quality of the analyses. True measures of the analysis quality require verifications against independent observations or verification of subsequent forecasts, which will be presented later.

Figure 8b shows the fit of the analysis and forecast MSLPs to the best-track data from the National Hurricane Center. The best-track MSLP is more or less constant during this 3-h period, being at about 952 hPa. At the beginning of DA cycling (0000 UTC 13 September), the MSLP is about 23 hPa higher than the best-track estimate. Most of the reductions in MSLP in all cases are actually achieved through adjustment during the forecasting process, with more than 15-hPa reduction achieved during the first analysis cycle between 0000 and 0030 UTC. This is not surprising because wind is the only parameter directly measured, and pressure analysis increments are only achieved through balance relationships and/or cross covariance, which are apparently weak.

We note in general, the MSLP decreases faster in the short forecasts between the analyses in the hybrid experiments than in 3DVARb. This is consistent with the fact that the hybrid method tends to build a warmer vortex core, and warmer temperature tends to induce a lower surface pressure due to hydrostatic balance. A stronger vortex circulation will also induce lower central pressure due to cyclostrophic balance. During the final three cycles, there is clearly overdeepening of the central pressure in HybridH in the short forecasts, resulting in a fall of MSLP that is about 5.5 hPa too low compared to best track. The final analyzed MSLP in HybridF is about 2.0 hPa too low, which should be within the uncertainty range of MSLP best-track data. We also note that in this study, since the dense radar data define the TC center location rather well (Fig. 3) and are assimilated every 30 min, the TC locations in the first-guess ensembles do not diverge too much in the 30-min forecasts throughout the assimilation cycles.

Overall, errors in the maximum surface wind (MSW) and MSLP are greatly reduced after assimilating radar data in all DA experiments. At 0300 UTC 13 September, the end of the DA cycles, the best-track MSW and MSLP are 47.5 m s^{-1} and 951 hPa, respectively. For 3DVARb, HybridF, and HybridH, after assimilating

radar radial wind, the MSW errors are 1, 0.8, and 2.7 m s^{-1} and the MSLP errors are 0.2, 1.9, and 5.6 hPa, respectively. The larger MSW (which is not directly observed) error in HybridH suggests that there is overfitting of the analyzed wind to Vr observations (Fig. 8a). For the NoDA experiment without assimilating radar data, the MSW error is 9 m s^{-1} and MSLP error is 29 hPa.

e. *The analyzed hurricane structures*

We examine next the structure of the hurricane at the end of the DA cycles by plotting fields at the surface and in vertical cross sections through the analyzed hurricane center. Figure 9 shows the analyzed mean sea level pressure and surface wind vectors for NoDA, 3DVARb, HybridF, and HybridH. Compared with NoDA (Fig. 9a), the analyzed vortex circulations are stronger and the minimum sea level pressure is much lower in 3DVARb, HybridF, and HybridH (Figs. 9b–d). Such primary hurricane circulations (Willoughby 1990) are captured well by the assimilation of radar radial velocity data.

Figure 10 shows the vertical cross sections of horizontal wind speed and potential temperature for all four experiments. The locations of cross sections, which are through the analyzed hurricane center and the location of maximum wind speed of each experiment, are indicated by the thick lines in Fig. 9; the locations of MSLP and maximum wind for the four experiments are slightly different. In NoDA, the hurricane eye is much wider and the intensity is much weaker than in the three radar DA experiments. Unlike the hybrid experiments, the potential temperature contours of 3DVARb (Fig. 10b) do not bend downward below ~ 600 hPa. The downward extrusion of potential temperature contours in HybridF and HybridH indicates a warm core structure (Figs. 10c,d). In experiment 3DVARb (Fig. 10b), the maximum wind speed at ~ 850 hPa on the right side of eyewall is about 10 m s^{-1} larger than those in HybridF and HybridH (Figs. 10c,d), but this larger wind speed is not accompanied by a warmer core expected of a stronger TC; this is an indication that the 3DVAR analysis is not dynamically and thermodynamically balanced.

Given the inner eye pressure deficit, the warm core should extend through the depth of the troposphere based on the hydrostatic approximation (Haurwitz 1935). The warm core structure is seen clearly in the vertical cross sections of horizontal temperature anomaly, which is the deviation from the mean at the pressure levels (Fig. 11). The temperature anomaly in NoDA is very small (less than 2 K; Fig. 11a) while that in 3DVARb, HybridF, and HybridH exceeds 8 K, with the maximum anomaly found between 300- and 500-hPa levels (Figs. 11b–d). This result is consistent with observational studies; the strength of the hurricane warm core

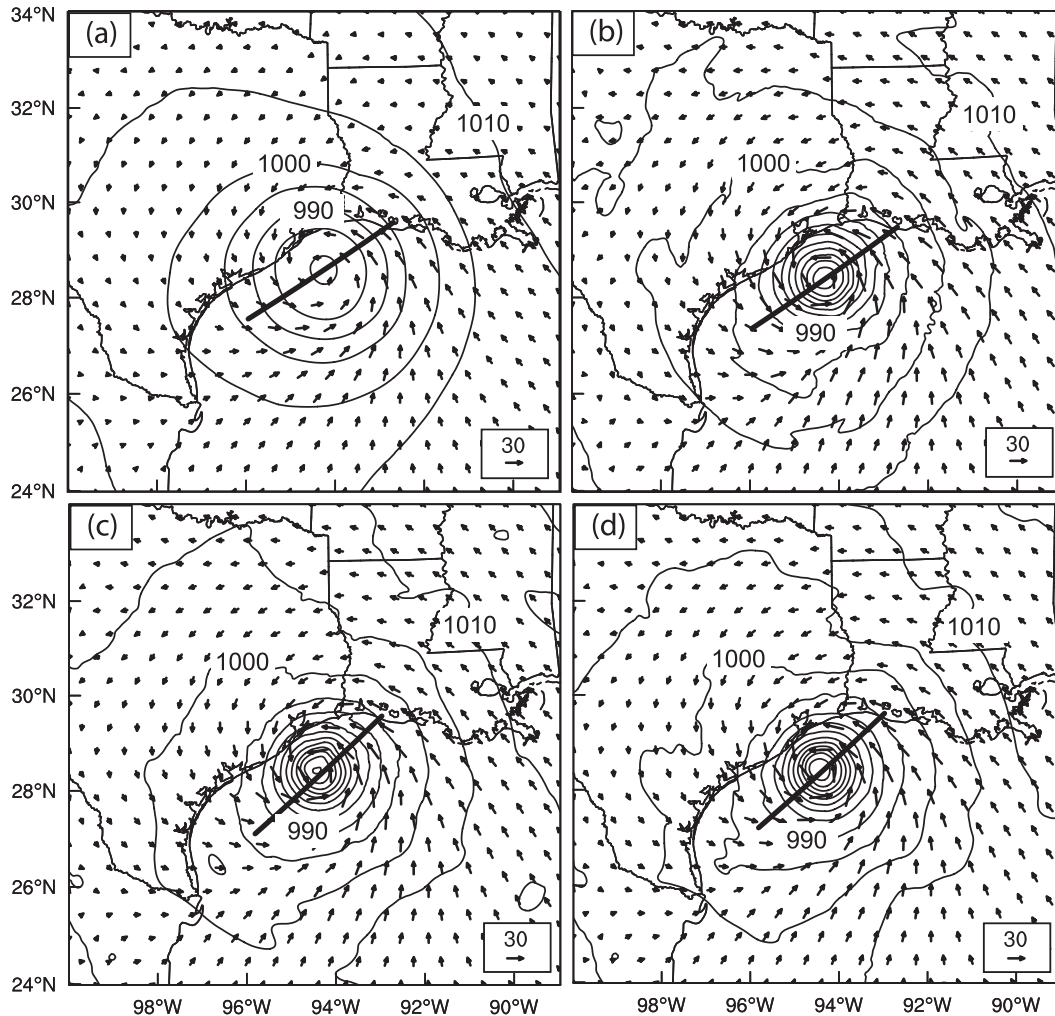


FIG. 9. The analyzed sea level pressure (interval of 5 hPa, solid contours) and the surface wind vectors (m s^{-1}) for (a) NoDA, (b) 3DVARb, (c) HybridF, and (d) HybridH at 0300 UTC 13 Sep 2008. The thick solid line indicates the vertical cross-sectional location in Figs. 10 and 11.

has been shown to negatively correlate with MSLP (Halverson et al. 2006; Hawkins and Imbembo 1976).

The near-zero or negative temperature anomaly below 700 hPa is clear in Fig. 11b for 3DVARb. This is related to the negative 3DVARb temperature increment discussed earlier. It is worth noting that the 3DVARb analysis does produce a reasonable warm core aloft. In HybridF and HybridH, the positive anomaly extends to the surface (Figs. 11c,d). In the latter two, the maximum anomaly is found to be at the inner edge of hurricane eyewall at about 400 hPa, which should be associated with the eyewall warming (LaSeur and Hawkins 1963; Holland 1997).

f. The track and intensity forecasts

To further evaluate the quality of analyses produced by different DA methods, deterministic forecasts initialized

from the (ensemble mean in the hybrid cases) analyses at 0300 UTC 13 September, the end of the DA cycles, are launched. The track forecasts are compared in Fig. 12a. The center of the hurricane is defined as the location of MSLP. The initial track errors at 0300 UTC are less than 20 km for all four experiments. By 0000 UTC 14 September, the track errors are 98, 117, 84, and 64 km for NoDA, 3DVARb, HybridF, and HybridH, respectively. The mean track errors based on the hurricane positions at 6-h interval during the period from 0300 UTC 13 September to 0000 UTC 14 September are 41, 57, 41, and 34 km for NoDA, 3DVARb, HybridF, and HybridH, respectively. Given that our DA experiments do not include environmental observations, the main effect on the track should come from the changes to the structure and intensity of the analyzed hurricane.

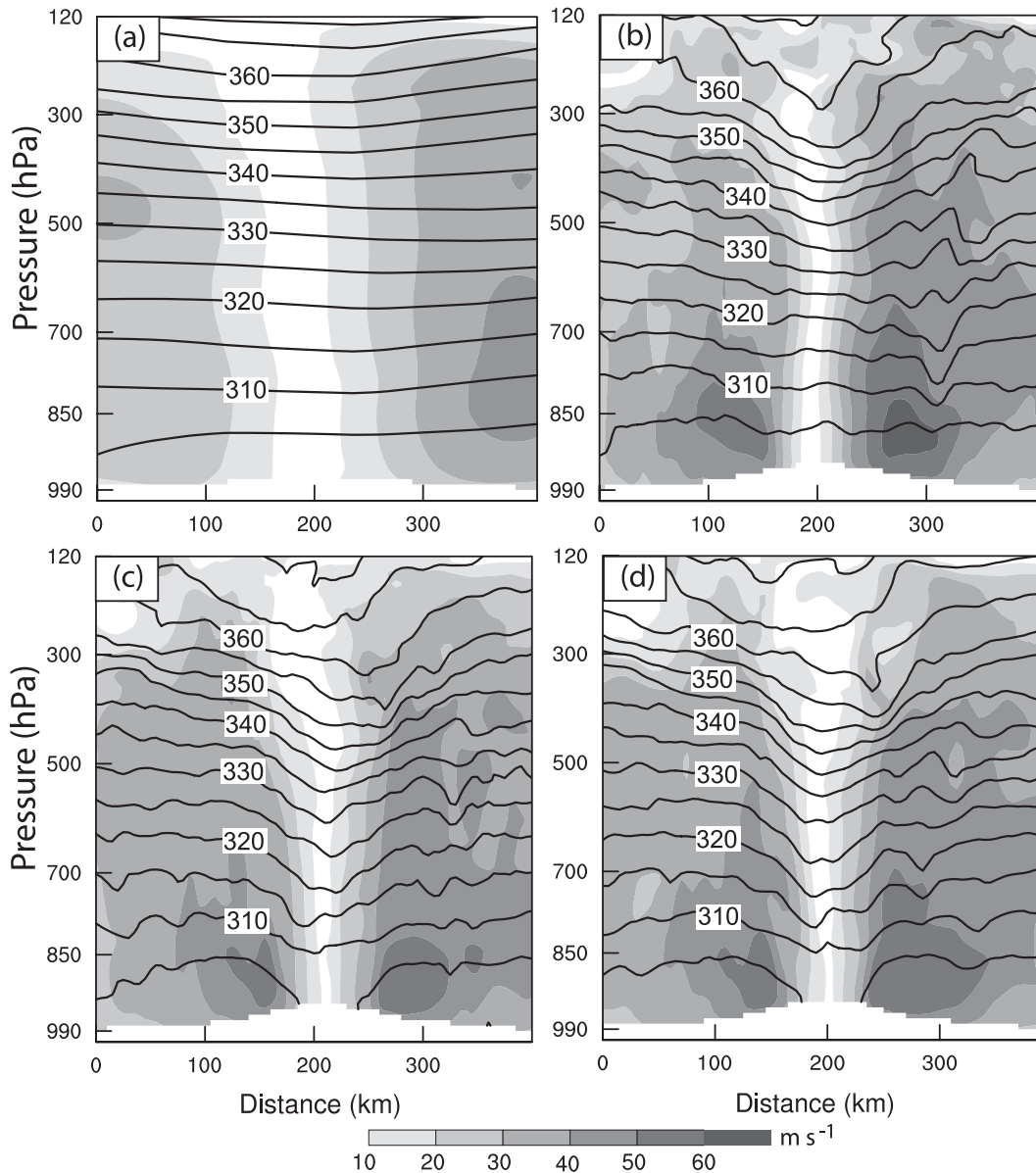


FIG. 10. Vertical cross sections of analyzed horizontal wind speed (interval of 10 m s^{-1} , shaded) and potential temperature (interval of 5 K , solid contours) for (a) NoDA, (b) 3DVARb, (c) HybridF, and (d) HybridH at 0300 UTC 13 Sep 2008.

Figure 12b shows the intensity forecasts in terms of MSLP, together with the best-track MSLP. At 0300 UTC 13 September, the MSLP errors are 28, 0.2, 2.0, and 5.5 hPa for NoDA, 3DVARb, HybridF, and HybridH, respectively. NoDA has the largest MSLP error throughout the forecast. The MSLP error in 3DVARb is smaller at the initial time, but becomes larger than those of HybridF and HybridH at the later forecast times. Overall, the forecast MSLP in the two hybrid experiments is closer to the best-track MSLP than that of 3DVARb. None of the forecasts capture the slight deepening during the first 3 h of forecast.

g. Verification of forecasts against Vr observations

The wind forecasts are further verified against observed radar radial velocity data. Figure 13 shows the root-mean-square errors (RMSEs, strictly it is RMSD because observations also contain error) of forecast against observed Vr for 3DVARb, HybridF, and HybridH. Compared to the best-track estimation of wind speed, the radar Vr observations are more reliable. At the initial time of 0300 UTC, the RMSE of 3.5 m s^{-1} from HybridF is slightly larger than those from HybridH (2.6 m s^{-1}) and 3DVARb (2.8 m s^{-1}). After the first

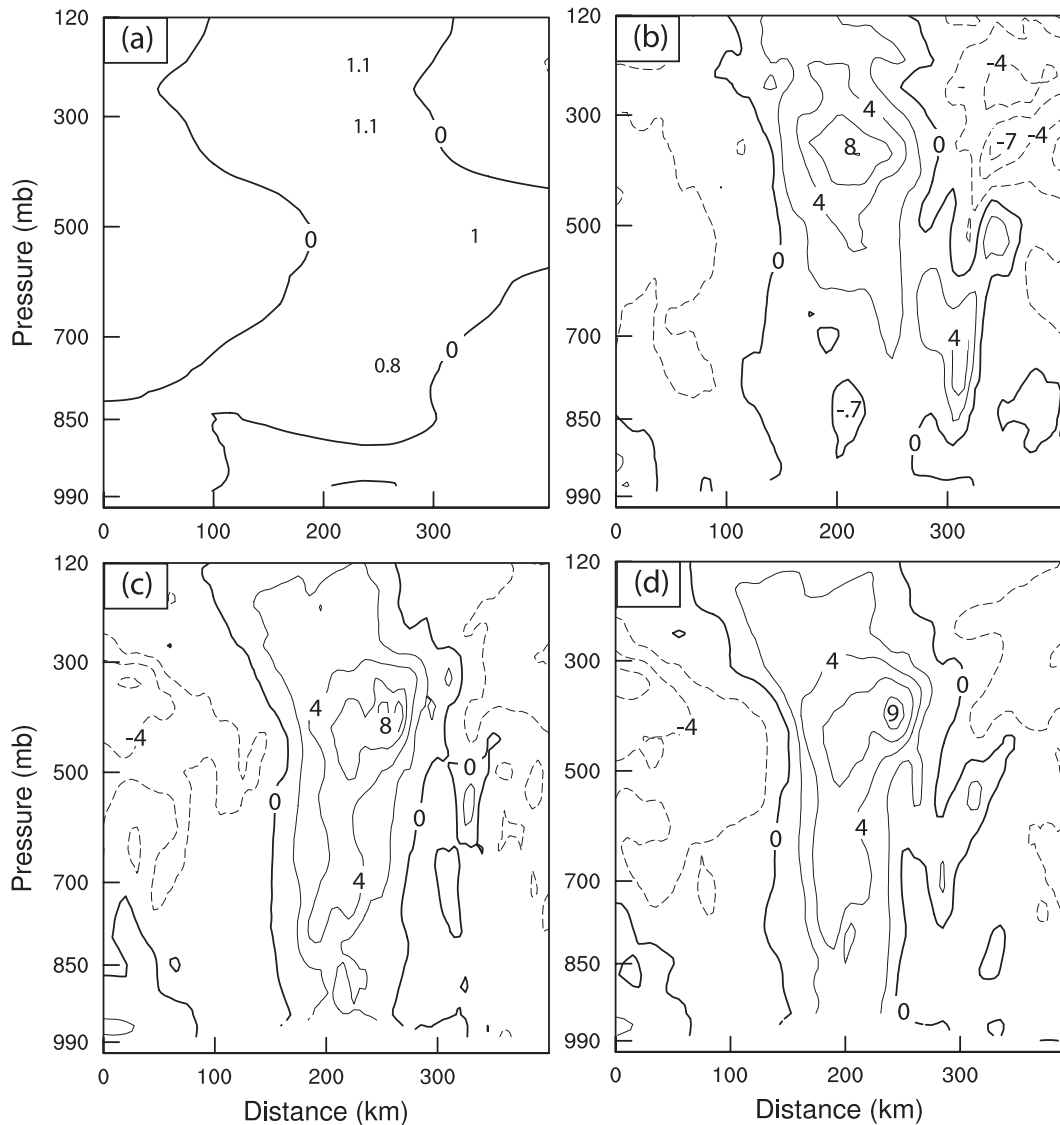


FIG. 11. Vertical cross sections of analyzed temperature anomalies (interval of 2 K) for (a) NoDA, (b) 3DVARb, (c) HybridF, and (d) HybridH at 0300 UTC 13 Sep 2008.

hour, the HybridF wind forecast fits the observed radial wind best, especially after 6 h of forecast where the error in 3DVARb grows much faster reaching 14.8 m s^{-1} compared to $8\text{--}9 \text{ m s}^{-1}$ in the hybrid cases. The much faster error growth in 3DVARb, even though its fit to V_r observations at the start of free forecast is comparable to that of HybridH and better than HybridF, again suggests that other model fields in the 3DVARb analysis are dynamically less consistent with the wind field than in the hybrid cases. As shown in Fig. 7, major differences exist between the 3DVAR and hybrid methods with the cross variable updating. This is further confirmed with the performance of HybridH in Fig. 13. Even though the HybridH analysis

is even more overfitting to observations than the 3DVAR (Fig. 8a), the forecast of HybridH was better than the 3DVAR because of the use of ensemble covariance. Interestingly, this overfitting to conventional temperature and wind observations in 3DVAR analysis and worse fitting to observations in the forecast, compared with hybrid where the forecast ensemble perturbations were used to estimate background error covariance, is also seen in other studies with quite different application (Fig. 2 of Wang et al. 2008b). The slightly better forecast in HybridF than in HybridH at 6 h suggests that the fully flow-dependent covariance during the assimilation cycles is beneficial.

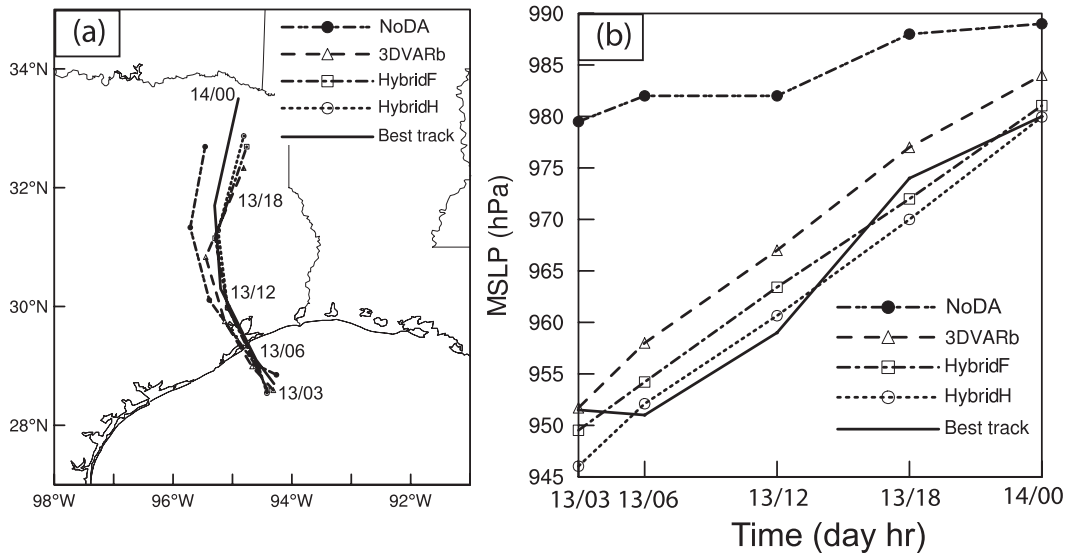


FIG. 12. Deterministic forecast hurricane (a) tracks and (b) minimum sea level pressure (hPa) by NoDA, 3DVARb, HybridF, and HybridH as compared to NHC best-track estimates from 0300 UTC 13 Sep through 0000 UTC 14 Sep 2008.

h. Evaluation of rainfall forecasts

Rainfall forecasts are evaluated by calculating equitable threat scores (ETSs) of 3-h accumulated precipitation against NCEP Stage-IV precipitation analyses (Fig. 14). For the thresholds of 5, 10, and 25 mm (3 h)⁻¹ and all forecast lead times, the hybrid experiments have higher ETSs than 3DVARb. Furthermore, the improvement of the hybrid over 3DVARb increases with precipitation threshold, indicating again the superior quality of the hybrid DA method. In addition, HybridF has slightly higher ETS scores than HybridH for most times and thresholds. The ETS of the hybrid experiments is higher than the NoDA for larger threshold and longer forecast lead times. By further looking at the precipitation patterns, it is found that the precipitation forecasts of HybridF more closely match the observed convective spiral band patterns in the inner-core region while 3DVARb produces too much precipitation in the southeast quadrant in the outer-band region (the region is within the reflectivity coverage of coastal radars, from which the Stage-IV precipitation is estimated; cf. Fig. 1) and the radius of the inner-core eyewall appears larger than observed (Fig. 15). In comparison, the precipitation pattern from the NoDA case is poorer than the DA experiments especially for inner rainbands. We do note that during the earlier hours and for lower thresholds, the ETSs of NoDA are comparable to those of hybrid schemes and higher than those of 3DVARb. The exact cause is difficult to ascertain. Imbalances and adjustments in the 3DVAR

analyses with short analysis-forecast cycles might have been a cause for the poorer performance, but this is only a hypothesis.

5. Summary and conclusions

In this study, the WRF hybrid ensemble-3DVAR data assimilation (DA) system is applied for the first time to the assimilation of radial velocity data for a

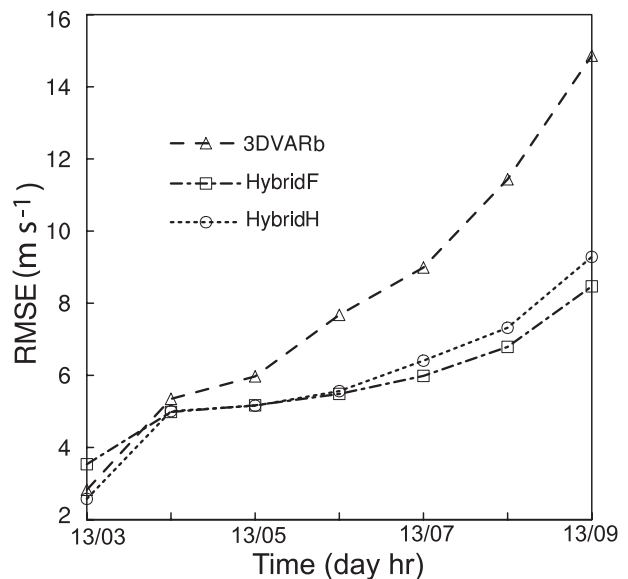


FIG. 13. Deterministic forecast RMSEs of V_r (m s^{-1}) by 3DVARb, HybridF, and HybridH from 0300 to 0900 UTC 13 Sep 2008.

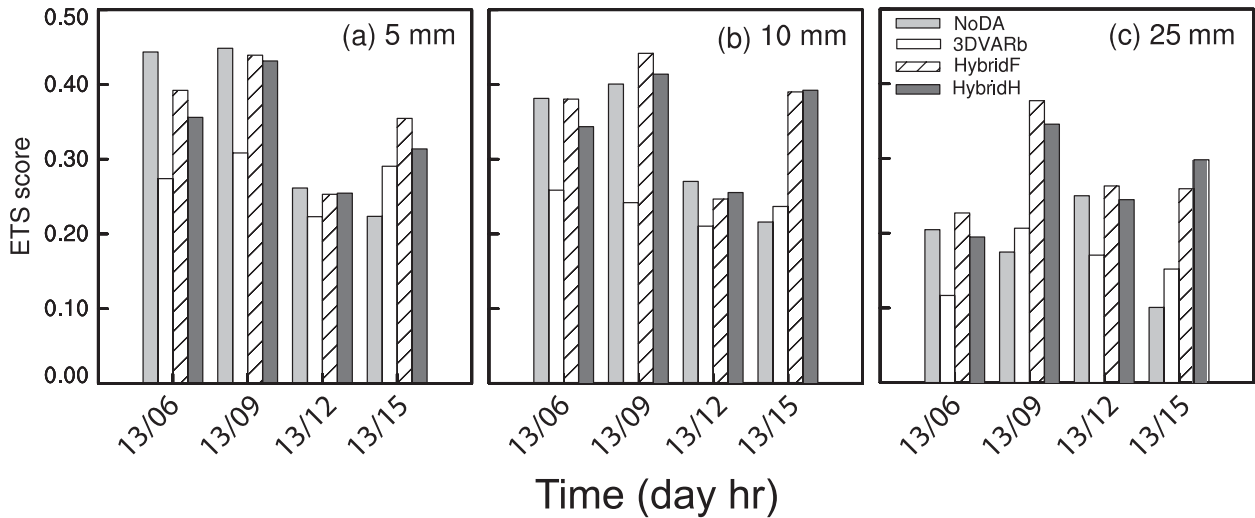


FIG. 14. ETSs for 3-h accumulated forecast precipitation by NoDA, 3DVARb, HybridF, and HybridH at thresholds (a) 5, (b) 10, and (c) 25 mm verified against NCEP Stage-IV precipitation analyses valid at 0600, 0900, 1200, and 1500 UTC 13 Sep 2008.

landfalling hurricane. More specifically, radial velocity data from two operational WSR-88D radars along the Gulf of Mexico coast are assimilated over a 3-h period after Hurricane Ike (2008) moved into the coverage of the two radars, using an enhanced version of the WRF hybrid DA system. Instead of using an ensemble transformation Kalman filter as in an earlier study to

generate the analysis ensemble, we employ in this study the “perturbed observation” method. Further, we applied vertical localization based on empirical orthogonal functions while continuing to use recursive filters for horizontal localization for the flow-dependent ensemble-estimated background error covariance. The flow-dependent ensemble covariance is incorporated

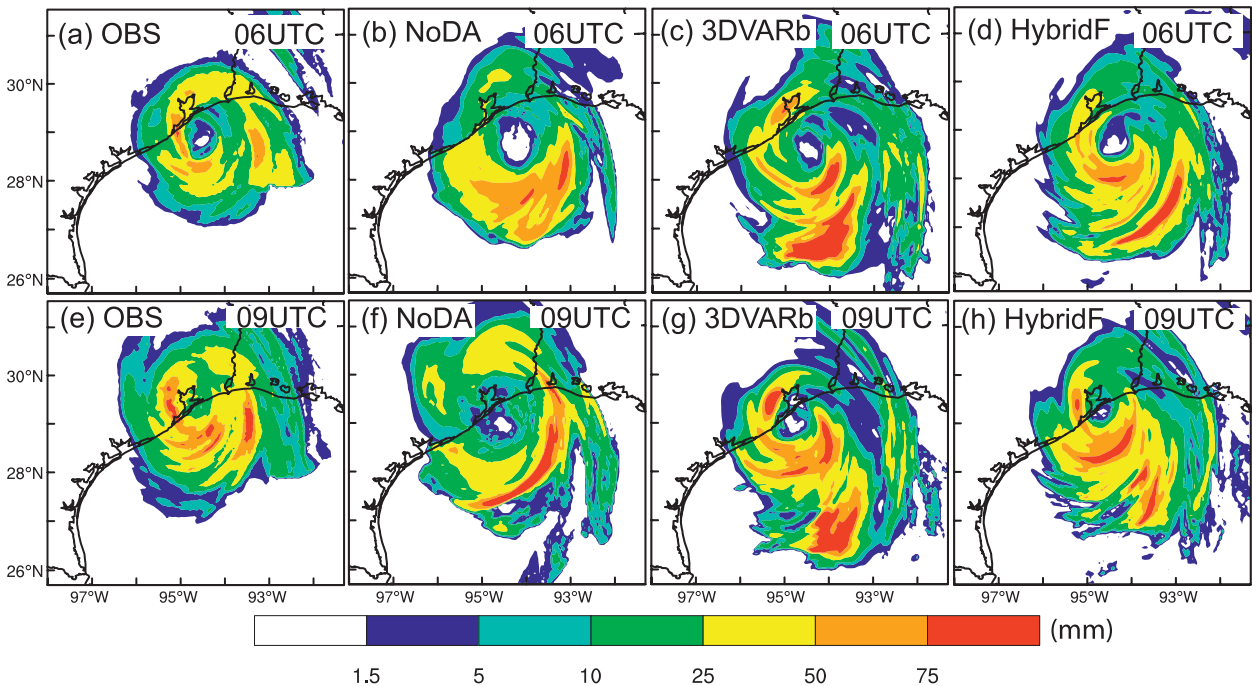


FIG. 15. The 3-h accumulated precipitation (mm) by (from left to right) NCEP Stage-IV precipitation analyses, NoDA, 3DVARb, and HybridF valid at (top) 0600 and (bottom) 0900 UTC 13 Sep 2008.

into the 3D variational framework by using the extended control variable method.

The radial velocity data are assimilated every 30 min over a 3-h period. Results mainly from five experiments are presented. A forecast experiment without assimilating any radar data is first carried out to serve as a baseline against which the radar-assimilating experiments are compared; this forecast experiment (NoDA) started directly from the operational GFS analysis, which contained too weak a hurricane vortex. The four radar DA experiments used the WRF 3DVAR using the static covariance derived from the NMC method (3DVARa), the WRF 3DVAR using further tuned static covariance (3DVARb), the hybrid DA system with purely flow-dependent background covariance (HybridF), as well as half static and half flow-dependent covariance (HybridH), respectively. In the tuned 3DVAR experiment (3DVARb) as well as HybridH, the horizontal spatial correlation scale in the static covariance derived from the NMC method is reduced by a factor of 0.3 to produce much more realistic wind increments than the default scale (in 3DVARa). The results of analyses and forecasts from the five experiments are intercompared and verified against best-track data, radar wind measurements, and precipitation data. The main conclusions are summarized in the following:

- 1) HybridF produces the most realistic temperature increments with positive values at the hurricane center, corresponding to the warm core structure, while 3DVARb produces much weaker and smoother temperature increments that are negative at the center of hurricane. At the end of assimilation cycles, negative temperature anomalies are found at lower levels in the eye region of 3DVARb analysis, while the hybrid analyses show deep warm core structures.
- 2) All three DA experiments are able to create analyses that fit the Vr data well, and the error reduction by analysis is the largest in the first analysis cycle. Most of the minimum sea level pressure (MSLP) reduction is achieved through model adjustment during the forecast step of the assimilation cycles
- 3) The hybrid experiments improve the Ike track forecast slightly, over the track forecast by NoDA starting from the GFS analysis. 3DVARb slightly degrades the track forecast. All radar DA experiments produce MSLP forecasts closer to the best-track observation than NoDA does.
- 4) The fit of forecast radial velocity to radar observations of 3DVARb is much worse than those of HybridF and HybridH. The forecast results indicate that the overall quality of hybrid analyses is better than that of 3DVARb, producing more dynamically

consistent state estimations that lead to later slower error growth during forecast. The forecast error of HybridF is slightly lower than that of HybridH starting from hour three.

- 5) The equitable threat scores (ETs) for 3-h accumulated precipitation forecasts in the hybrid experiments are higher than those of 3DVARb for the thresholds and lead times considered, and the improvement increases with precipitation threshold, indicating again the superior quality of the hybrid DA method. Among the hybrid experiments, HybridF produced slightly better ETs than HybridH at most verification times.
- 6) The results of this study also show positive impacts of assimilating radar data for hurricane initialization, and the hybrid-method-analyzed hurricane has kinematic and thermodynamic structures that are consistent with tropical cyclone conceptual models.

Finally a point worth noting: the inclusion of static background covariance in HybridH in general did not improve the results over HybridF in this case study (i.e., the use of flow-dependent covariance in full in general gives better results). Earlier studies (Hamill and Snyder 2000; Wang et al. 2007a) suggested that the optimal combination of the static and flow-dependent covariance depends on their relative quality. The results in this case study suggest that for hurricanes and radar data, there is likely little benefit of including static covariance because the static covariance is not capable of appropriately reflecting the mesoscale and convective-scale nature of hurricanes.

We also note that this study represents the first attempt of applying a variational-ensemble hybrid data assimilation method to hurricane and radar data assimilation. While the results are positive and encouraging, more robust conclusions will need to be drawn by testing the method on many more cases.

Acknowledgments. This research was primarily supported by a subcontract to a grant from the Mississippi State University led by Dr. Haldun Karan. The first author also acknowledges Dr. Curtis N. James for radar data processing, and Shizhang Wang, Alex Schenkman, and Dr. Robin Tanamachi for helpful discussions and assistance with initial drafts. This work was also supported by NSF Grant AGS-0802888, DOD-ONR Grant N00014-10-1-0775, NOAA THOPREX Grant NA08OAR4320904, NASA NIP Grant NNX10AQ78G, and NOAA HFIP Grant NA12NWS4680012. The experiments were conducted on a supercomputer at the Mississippi State University.

REFERENCES

- Aksoy, A., S. Lorsolo, T. Vukicevic, K. J. Sellwood, S. D. Abersson, and F. Zhang, 2012: The HWRF Hurricane Ensemble Data Assimilation System (HEDAS) for high-resolution data: The impact of airborne Doppler radar observations in an OSSE. *Mon. Wea. Rev.*, **140**, 1843–1862.
- Barker, D. M., W. Huang, Y. R. Guo, A. J. Bourgeois, and Q. N. Xiao, 2004: A three-dimensional variational data assimilation system for MM5: Implementation and initial results. *Mon. Wea. Rev.*, **132**, 897–914.
- Blake, E. S., C. W. Landsea and E. J. Gibney, 2011: The deadliest, costliest, and most intense United States tropical cyclones from 1851 to 2010 (and other frequently requested hurricane facts). NOAA Tech. Memo. NWS NHC-6, National Hurricane Center, Miami, FL, 49 pp. [Available online at <http://www.nhc.noaa.gov/pdf/nws-nhc-6.pdf>.]
- Buehner, M., 2005: Ensemble-derived stationary and flow-dependent background-error covariances: Evaluation in a quasi-operational NWP setting. *Quart. J. Roy. Meteor. Soc.*, **131**, 1013–1043.
- , P. L. Houtekamer, C. Charette, H. L. Mitchell, and B. He, 2010a: Intercomparison of variational data assimilation and the ensemble Kalman filter for global deterministic NWP. Part I: Description and single-observation experiments. *Mon. Wea. Rev.*, **138**, 1550–1566.
- , —, —, —, and —, 2010b: Intercomparison of variational data assimilation and the ensemble Kalman filter for global deterministic NWP. Part II: One-month experiments with real observations. *Mon. Wea. Rev.*, **138**, 1567–1586.
- Burgers, G., P. J. van Leeuwen, and G. Evensen, 1998: Analysis scheme in the ensemble Kalman filter. *Mon. Wea. Rev.*, **126**, 1719–1724.
- Dong, J., and M. Xue, 2012: Coastal WSR-88D radar data assimilation with ensemble Kalman filter for analysis and forecast of Hurricane Ike (2008). *Quart. J. Roy. Meteor. Soc.*, doi:10.1002/qj.1970, in press.
- Dowell, D. C., and L. J. Wicker, 2009: Additive noise for storm-scale ensemble data assimilation. *J. Atmos. Oceanic Technol.*, **26**, 911–927.
- Dudhia, J., 1989: Numerical study of convection observed during the Winter Monsoon Experiment using a mesoscale two-dimensional model. *J. Atmos. Sci.*, **46**, 3077–3107.
- Etherton, B. J., and C. H. Bishop, 2004: The resilience of hybrid ensemble/3D-Var analysis schemes to model error and ensemble covariance error. *Mon. Wea. Rev.*, **132**, 1065–1080.
- Evensen, G., 2003: The ensemble Kalman filter: Theoretical formulation and practical implementation. *Ocean Dyn.*, **53**, 343–367.
- Grell, G. A., and D. Devenyi, 2002: A generalized approach to parameterizing convection combining ensemble and data assimilation techniques. *Geophys. Res. Lett.*, **29**, 1693, doi:10.1029/2002GL015311.
- Halverson, J. B., J. Simpson, G. Heymsfield, H. Pierce, T. Hock, and L. Ritchie, 2006: Warm core structure of Hurricane Erin diagnosed from high-altitude dropsondes during CAMEX-4. *J. Atmos. Sci.*, **63**, 309–324.
- Hamill, T. M., and C. Snyder, 2000: A hybrid ensemble Kalman filter-3D variational analysis scheme. *Mon. Wea. Rev.*, **128**, 2905–2919.
- , J. S. Whitaker, M. Fiorino, and S. G. Benjamin, 2011: Global ensemble predictions of 2009's tropical cyclones initialized with an ensemble Kalman filter. *Mon. Wea. Rev.*, **139**, 668–688.
- Haurwitz, B., 1935: The height of tropical cyclones and the eye of the storm. *Mon. Wea. Rev.*, **63**, 45–49.
- Hawkins, H. F., and S. M. Imbembro, 1976: The structure of a small, intense hurricane—Inez 1966. *Mon. Wea. Rev.*, **104**, 418–442.
- Holland, G. J., 1997: The maximum potential intensity of tropical cyclones. *J. Atmos. Sci.*, **54**, 2519–2541.
- Hong, S.-Y., J. Dudhia, and S.-H. Chen, 2004: A revised approach to ice microphysical processes for the bulk parameterization of clouds and precipitation. *Mon. Wea. Rev.*, **132**, 103–120.
- Houtekamer, P. L., and H. L. Mitchell, 1998: Data assimilation using an ensemble Kalman filter technique. *Mon. Wea. Rev.*, **126**, 796–811.
- Hu, M., M. Xue, J. Gao, and K. Brewster, 2006: 3DVAR and cloud analysis with WSR-88D level-II data for the prediction of Fort Worth tornadic thunderstorms. Part II: Impact of radial velocity analysis via 3DVAR. *Mon. Wea. Rev.*, **134**, 699–721.
- James, C. N., and R. A. Houze, 2001: A real-time four-dimensional Doppler dealiasing scheme. *J. Atmos. Oceanic Technol.*, **18**, 1674–1683.
- Kleist, D., K. Ide, J. Whitaker, J. C. Derber, D. Parrish, and X. Wang, 2011: Expanding the GSI-based hybrid ensemble-variational system to include more flexible parameter settings. Preprints, *15th Symp. on Integrated Observing and Assimilation Systems for the Atmosphere, Oceans and Land Surface (IOAS-AOLS)*, Seattle, WA, Amer. Meteor. Soc., J16.4. [Available online at <https://ams.confex.com/ams/91Annual/webprogram/Paper180096.html>.]
- Kurihara, Y., M. A. Bender, R. E. Tuleya, and R. Ross, 1995: Improvements in the GFDL hurricane prediction system. *Mon. Wea. Rev.*, **123**, 2791–2801.
- La Seur, N. E., and H. F. Hawkins, 1963: An analysis of Hurricane Cleo (1958) based on data from research reconnaissance aircraft. *Mon. Wea. Rev.*, **91**, 694–709.
- Li, J., and H. Liu, 2009: Improved hurricane track and intensity forecast using single field-of-view advanced IR sounding measurements. *Geophys. Res. Lett.*, **36**, L11813, doi:10.1029/2009GL038285.
- Liu, C., Q. Xiao, and B. Wang, 2008: An ensemble-based four-dimensional variational data assimilation scheme. Part I: Technical formulation and preliminary test. *Mon. Wea. Rev.*, **136**, 3363–3373.
- , —, and —, 2009: An ensemble-based four-dimensional variational data assimilation scheme. Part II: Observing System Simulation Experiments with Advanced Research WRF (ARW). *Mon. Wea. Rev.*, **137**, 1687–1704.
- Liu, Q., T. Marchok, H.-L. Pan, M. Bender, and S. J. Lord, 2000: Improvements in hurricane 2 initialization and forecasting at NCEP with global and regional (GFDL) models. Tech. Rep. 3, NOAA Tech. Procedures Bull. 472, 7 pp.
- Liu, S., M. Xue, J. Gao, and D. Parrish, 2005: Analysis and impact of super-obbed Doppler radial velocity in the NCEP Grid-point Statistical Interpolation (GSI) analysis system. Preprints, *21st Conf. on Weather Analysis and Forecasting/17th Conf. on Numerical Weather Prediction*, Washington, DC, Amer. Meteor. Soc., 13A.4. [Available online at https://ams.confex.com/ams/WAFNWP34BC/techprogram/paper_94230.htm.]
- Lorenc, A., 2003: The potential of the ensemble Kalman filter for NWP—A comparison with 4D-Var. *Quart. J. Roy. Meteor. Soc.*, **129**, 3183–3204.
- Mlawer, E. J., S. J. Taubman, P. D. Brown, M. J. Iacono, and S. A. Clough, 1997: Radiative transfer for inhomogeneous atmospheres: RRTM, a validated correlated-k model for the longwave. *J. Geophys. Res.*, **102** (D14), 16 663–16 682.

- Noh, Y., W. G. Cheon, S. Y. Hong, and S. Raasch, 2003: Improvement of the K-profile model for the planetary boundary layer based on large eddy simulation data. *Bound.-Layer Meteor.*, **107**, 401–427.
- Parrish, D. F., and J. C. Derber, 1992: The National Meteorological Center's spectral statistical-interpolation analysis system. *Mon. Wea. Rev.*, **120**, 1747–1763.
- Pielke, R. A., J. Gratz, C. W. Landsea, D. Collins, M. A. Saunders, and R. Musulin, 2008: Normalized hurricane damage in the United States: 1900–2005. *Nat. Hazards Rev.*, **9**, 29–42.
- Schenkman, A., M. Xue, A. Shapiro, K. Brewster, and J. Gao, 2011: The analysis and prediction of the 8–9 May 2007 Oklahoma tornadic mesoscale convective system by assimilating WSR-88D and CASA radar data using 3DVAR. *Mon. Wea. Rev.*, **139**, 224–246.
- Skamarock, W. C., and Coauthors, 2008: A description of the Advanced Research WRF version 3. NCAR Tech. Note TN-475+STR, 113 pp.
- Sugimoto, S., N. A. Crook, J. Sun, Q. Xiao, and D. Barker, 2009: Assimilation of Doppler radar data with WRF 3DVAR: Evaluation of its potential benefits to quantitative precipitation forecasting through Observing System Simulation Experiments. *Mon. Wea. Rev.*, **137**, 4011–4029.
- Torn, R. D., and G. J. Hakim, 2009: Initial condition sensitivity of western Pacific extratropical transitions determined using ensemble-based sensitivity analysis. *Mon. Wea. Rev.*, **137**, 3388–3406.
- , —, and C. Snyder, 2006: Boundary conditions for limited-area ensemble Kalman filters. *Mon. Wea. Rev.*, **134**, 2490–2502.
- Wang, X., 2010: Incorporating ensemble covariance in the Grid-point Statistical Interpolation (GSI) variational minimization: A mathematical framework. *Mon. Wea. Rev.*, **138**, 2990–2995.
- , 2011: Application of the WRF hybrid ETKF-3DVAR data assimilation system for hurricane track forecasts. *Wea. Forecasting*, **26**, 868–884.
- , T. M. Hamill, J. S. Whitaker, and C. H. Bishop, 2007a: A comparison of hybrid ensemble transform Kalman filter-OI and ensemble square-root filter analysis schemes. *Mon. Wea. Rev.*, **135**, 1055–1076.
- , C. Snyder, and T. M. Hamill, 2007b: On the theoretical equivalence of differently proposed ensemble/3D-Var hybrid analysis schemes. *Mon. Wea. Rev.*, **135**, 222–227.
- , D. M. Barker, C. Snyder, and T. M. Hamill, 2008a: A hybrid ETKF-3DVAR data assimilation scheme for the WRF model. Part I: Observing System Simulation experiment. *Mon. Wea. Rev.*, **136**, 5116–5131.
- , —, —, and —, 2008b: A hybrid ETKF-3DVAR data assimilation scheme for the WRF model. Part II: Real observation experiment. *Mon. Wea. Rev.*, **136**, 5132–5147.
- , T. M. Hamill, J. S. Whitaker, and C. H. Bishop, 2009: A comparison of the hybrid and EnSRF analysis schemes in the presence of model error due to unresolved scales. *Mon. Wea. Rev.*, **137**, 3219–3232.
- , J. Whitaker, D. T. Kleist, D. F. Parrish, and B. W. Holland, 2011: A GSI-based hybrid ensemble-variational data assimilation system and its comparison with GSI and ensemble Kalman filter. Preprints, *15th Symp. on Integrated Observing and Assimilation Systems for the Atmosphere, Oceans and Land Surface (IOAS-AOLS)*, Seattle, WA, Amer. Meteor. Soc., J16.5. [Available online at <https://ams.confex.com/ams/91Annual/webprogram/Paper180532.html>.]
- Weng, Y., and F. Zhang, 2012: Assimilating airborne Doppler radar observations with an ensemble Kalman filter for convection-permitting hurricane initialization and prediction: Katrina (2005). *Mon. Wea. Rev.*, **140**, 841–859.
- , M. Zhang, and F. Zhang, 2011: Advanced data assimilation for cloud-resolving hurricane initialization and prediction. *Comput. Sci. Eng.*, **13**, 40–49.
- Whitaker, J., D. Kleist, X. Wang, and T. Hamill, 2011: Tests of a hybrid variational-ensemble data global assimilation system for hurricane prediction. Preprints, *15th Symp. on Integrated Observing and Assimilation Systems for the Atmosphere, Oceans and Land Surface (IOAS-AOLS)*, Seattle, WA, Amer. Meteor. Soc., J16.2. [Available online at <https://ams.confex.com/ams/91Annual/webprogram/Paper178847.html>.]
- Willoughby, H. E., 1990: Temporal changes in the primary circulation in tropical cyclones. *J. Atmos. Sci.*, **47**, 242–264.
- Xiao, Q. N., and J. Sun, 2007: Multiple radar data assimilation and short-range quantitative precipitation forecasting of a squall line observed during IHOP_2002. *Mon. Wea. Rev.*, **135**, 3381–3404.
- , X. Y. Zhang, C. Davis, J. Tuttle, G. Holland, and P. J. Fitzpatrick, 2009: Experiments of hurricane initialization with airborne Doppler radar data for the Advanced Research Hurricane WRF (AHW) model. *Mon. Wea. Rev.*, **137**, 2758–2777.
- Xu, Q., and J. D. Gong, 2003: Background error covariance functions for Doppler radial-wind analysis. *Quart. J. Roy. Meteor. Soc.*, **129**, 1703–1720.
- Zhang, F., C. Snyder, and J. Sun, 2004: Impacts of initial estimate and observations on the convective-scale data assimilation with an ensemble Kalman filter. *Mon. Wea. Rev.*, **132**, 1238–1253.
- , Y. Weng, J. A. Sippel, Z. Meng, and C. H. Bishop, 2009a: Cloud-resolving hurricane initialization and prediction through assimilation of Doppler radar observations with an ensemble Kalman filter. *Mon. Wea. Rev.*, **137**, 2105–2125.
- , M. Zhang, and J. A. Hansen, 2009b: Coupling ensemble Kalman filter with four-dimensional variational data assimilation. *Adv. Atmos. Sci.*, **26**, 1–8.
- , Y. Weng, J. F. Gamache, and F. D. Marks, 2011: Performance of convection-permitting hurricane initialization and prediction during 2008–2010 with ensemble data assimilation of inner-core airborne Doppler radar observations. *Geophys. Res. Lett.*, **38**, L15810, doi:10.1029/2011GL048469.
- Zhao, K., and M. Xue, 2009: Assimilation of coastal Doppler radar data with the ARPS 3DVAR and cloud analysis for the prediction of Hurricane Ike (2008). *Geophys. Res. Lett.*, **36**, L12803, doi:10.1029/2009GL038658.
- Zou, X. L., and Q. N. Xiao, 2000: Studies on the initialization and simulation of a mature hurricane using a variational bogus data assimilation scheme. *J. Atmos. Sci.*, **57**, 836–860.
- Zupanski, M., 2005: Maximum likelihood ensemble filter: Theoretical aspects. *Mon. Wea. Rev.*, **133**, 1710–1726.